HHS Public Access

Author manuscript

Cancer Discov. Author manuscript; available in PMC 2018 December 01.

Published in final edited form as:

Cancer Discov. 2017 December ; 7(12): 1450–1463. doi:10.1158/2159-8290.CD-17-0177.

mTOR and HDAC inhibitors converge on the TXNIP/thioredoxin pathway to cause catastrophic oxidative stress and regression of RAS-driven tumors

Clare F. Malone[1,2], **Chloe Emerson**[1,2], **Rachel Ingraham**[1,2], **William Barbosa**[1,2], **Stephanie Guerra**[1,2], **Haejin Yoon**[3], **Lin L. Liu**[4], **Franziska Michor**[4], **Marcia Haigis**[3], **Kay F. Macleod**[5], **Ophélia Maertens**[1,2,6], and **Karen Cichowski**[*,1,2,6]

[1]Genetics Division, Department of Medicine, Brigham and Women's Hospital, Boston, MA 02115, USA

[2]Harvard Medical School, Boston, MA 02115, USA

[3]Department of Cell Biology, Ludwig Center at Harvard, Harvard Medical School, Boston, MA 02115, USA

[4]Department of Biostatistics and Computational Biology, Dana-Farber Cancer Institute, Boston, MA 02115, USA

[5]The Ben May Institute for Cancer Research, The University of Chicago, Chicago, IL 60637, USA

[6]Ludwig Center at Harvard, Boston, MA 02115, USA

Abstract

While agents that inhibit specific oncogenic kinases have been successful in a subset of cancers, there are currently few treatment options for malignancies that lack a targetable oncogenic driver. Nevertheless, during tumor evolution cancers engage a variety of protective pathways, which may provide alternative actionable dependencies. Here we identify a promising combination therapy that kills *NF1*-mutant tumors by triggering catastrophic oxidative stress. Specifically, we show that mTOR and HDAC inhibitors kill aggressive nervous system malignancies and shrink tumors *in vivo* by converging on the TXNIP/thioredoxin anti-oxidant pathway, through cooperative effects on chromatin and transcription. Accordingly, TXNIP triggers cell death by inhibiting thioredoxin and activating Apoptosis Signal-regulating Kinase 1 (ASK1). Moreover, this drug combination also kills *NF1*-mutant and *KRAS*-mutant non-small cell lung cancers. Together these studies identify a promising therapeutic combination for several currently untreatable malignancies, and reveal a protective nodal point of convergence between these important epigenetic and oncogenic enzymes.

Keywords

NF1; RAS; mTOR; epigenetics; oxidative stress; combination therapy

[*]Correspondence: kcichowski@rics.bwh.harvard.edu; fax (617) 525-4705; phone (617) 525-4722.

There are no conflicts of interest to disclose.

Introduction

Genetic alterations in oncogenes and tumor suppressors play an important causal role in tumor development. Accordingly, therapeutic efforts have largely focused on identifying and inhibiting key oncogenic drivers and/or downstream pathways (1). However, in addition to accumulating mutations, cancers also activate a variety of protective pathways that are not sufficient to drive tumorigenesis, but are nonetheless characteristic of the tumorigenic state (2). As such, these cellular adaptations represent potential cancer-cell dependencies that could be exploited for therapeutic purposes (2). Strategies designed to inhibit these protective pathways may be particularly useful for treating tumors that are not driven by a readily targetable protein. The challenge has been to identify key nodal points within essential adaptive pathways, which may vary by tumor type and/or genotype.

Redox homeostasis is important for the survival of both normal and cancer cells (3). However, many tumors possess elevated levels of reactive oxygen species (ROS) and exhibit signs of chronic oxidative stress, which is caused by oncogenic insults, hypoxia, metabolic defects, and proteotoxic stress (4). At sub-lethal levels, increased ROS are thought to enhance tumor development by causing mutations and altering cell signaling (5). However, to prevent excessive oxidative damage, tumors frequently upregulate anti-oxidant pathways (5,6). Accordingly, many tumor cells are hypersensitive to perturbations in ROS levels (4). In fact, excessive oxidative stress is thought to contribute to the cytotoxic effects of chemotherapies and efforts to potentiate ROS production in these settings are underway (7,8). Nevertheless, because traditional cytotoxic agents also affect normal tissues, a targeted approach that selectively triggers catastrophic oxidative stress in tumor cells would offer a greater therapeutic window.

The *NF1* tumor suppressor encodes a RAS GTPase activating protein and is mutated in a familial cancer syndrome and in an expanding number of sporadic tumors (9–13). *NF1*-mutant malignancies are driven by excessive RAS signaling and, like *KRAS* mutant tumors, are largely unresponsive to current therapies (14). *NF1*-deficient nervous system tumors, known as MPNSTs (Malignant Peripheral Nerve Sheath Tumors), develop sporadically and in individuals with neurofibromatosis type I (NF1) and are lethal in approximately 70% of patients (15). Therefore new effective treatments are urgently needed.

The mTOR pathway has been shown to be critical in *NF1*-mutant malignancies (10,16). In addition to its well-documented role in cell growth, proliferation, and protein translation, mTOR also regulates the production of reduced glutathione (GSH), one of the three major cellular anti-oxidants: GSH, thioredoxin, and catalase (4). Specifically, mTOR regulates SREBP, a transcription factor that controls the production of glucose-6-phosphate dehydrogenase (G6PD), a rate-limiting enzyme in NADPH production and consequently glutathione reduction (17). Accordingly, mTOR inhibitors have been shown to suppress SREBP, G6PD, and GSH levels in MPNSTS (18). Nevertheless, mTOR inhibitors only exert cytostatic effects in these tumors (16,18,19). We therefore sought to identify other targeted agents that might cooperate with mTOR inhibitors to enhance oxidative stress beyond threshold levels, thereby killing these mTOR-driven malignancies. Here we show that HDAC and mTOR inhibitors together impinge on a second major anti-oxidant pathway, the

thioredoxin pathway, and trigger catastrophic oxidative stress, cell death, and most importantly tumor regression *in vivo*. Importantly, this combination also kills *NF1*-mutant and *KRAS*-mutant non-small cell lung cancers. Together these studies identify a promising new therapeutic combination for these RAS-driven tumors and reveal a cooperative mechanism of action that may be more generally exploited for the development of other therapies.

Results

HDAC and mTOR inhibitors cooperate to kill NF1-mutant nervous system malignancies

Because mTOR inhibitors suppress a major anti-oxidant pathway in MPNSTs, we sought to identify and combine other agents that stimulate ROS accumulation, as a potential strategy to induce catastrophic oxidative stress in these tumors. To facilitate clinical translation, we considered FDA-approved drugs that are known to enhance oxidative stress. Interestingly, HDAC inhibitors have been shown to elevate ROS in some tumor types (20). Indeed vorinostat, a pan histone-deacetylase (HDAC) inhibitor triggered an increase in ROS levels in human MPNST cells (Fig. 1A).

We then evaluated the combined effects of the mTOR kinase inhibitor, sapanisertib, and vorinostat in a variety of human MPNST cell lines and non-transformed cells. Sapanisertib was used because mTOR kinase inhibitors more effectively inhibit 4E-BP1 phosphorylation in these cells *in vitro* as compared to rapamycin (19), similar to observations in other cell lines (21,22), and because the 4E-BP/eIF4E pathway has been shown to be particularly important for MPNSTs (23). As previously reported, sapanisertib slowed the proliferation of MPNSTs, but cells did not die (23); however when combined, sapanisertib and vorinostat potently killed MPNSTs (Fig. 1B). Within 72 hours 59% of the cells died in response to this drug combination, whereas cells exposed to each agent alone continued to proliferate, albeit at a slower rate (Fig. 1B). These effects were observed in multiple MPNST cell lines and cell death was not dependent on the presence or absence of *p53* mutations (Fig. 1B and C and Supplementary Fig. S1A). Using the Gaddum's (non-) interaction score, which is the most appropriate method to evaluate synergy of a cytotoxic combination when at least one agent is cytostatic (24), these agents exerted synergistic effects on the reduction in cell number in MPNSTs (Supplementary Fig. S1B). In contrast, sapanisertib and vorinostat did not kill non-transformed cells, demonstrating that this combination is not generally toxic (Fig. 1D).

Combined HDAC and mTORC1 inhibitors trigger potent tumor regression in a genetically-engineered mouse tumor model

Before dissecting the molecular mechanism of action, we first investigated whether this combination was effective *in vivo*. Many putative therapies have been reported to slow the growth of tumors in animal models; however, targeted agents that are effective in the clinic, such as BRAF inhibitors in melanoma and EGFR inhibitors in lung cancer, cause frank tumor regression in preclinical studies (25,26). We therefore utilized a previously characterized genetically-engineered mouse model to determine whether this combination could shrink tumors *in vivo* (Fig. 1E and ref. 27). Similar to human tumors, MPNSTs that

develop in this model harbor null mutations in *Nf1* and *p53* and are histologically indistinguishable from human malignancies (27,28). Tumors develop with an average latency of 5 months and once detected grow rapidly in 10 days, mimicking the aggressive nature of human MPNSTs. Once palpable tumors were detected animals were randomized and treated with HDAC and/or mTOR inhibitors. In mice and humans rapalogues are able to suppress 4-EBP1 phosphorylation in many tissues (19,29), perhaps due to the long half-life of the drug and/or sequestration in immunophilin rich red blood cells *in vivo* (30). Because rapamycin (sirolimus) is FDA approved for other indications, we selected this agent for initial *in vivo* studies (19). Rapamycin, which exclusively suppresses mTORC1, effectively inhibited its activity *in vivo*, as demonstrated by the loss of the hyper-phosphorylated form of 4E-BP1 (Fig. 1F) and previously shown using both 4E-BP1 and phosphorylated S6 as pharmacodynamic biomarkers (19). The HDAC inhibitor vorinostat also effectively inhibited histone deacetylases *in vivo*, demonstrated by a sustained increase in acetylated H3K27 (Fig. 1F). Consistent with *in vitro* observations, vorinostat and rapamycin as single agents did not cause tumor regression; however, together they caused potent tumor shrinkage, on average by 38% and up to 76% with no signs of toxicity (Fig. 1G and Supplementary Fig. S2A). Notably, the dose of vorinostat used for this study (50 mg/kg), is predicted to be slightly less than the dose recently found to be tolerated when combined with rapamycin in humans (243 mg versus 300 mg), underscoring the translational potential of this finding (31).

Multiple mTOR and HDAC inhibitors recapitulate the therapeutic response

To confirm that the observed therapeutic effects were due to on-target suppression of mTOR and HDAC, we sought to evaluate additional agents. In order to select an appropriate HDAC inhibitor, we first performed *in vitro* studies. Vorinostat inhibits class I, II, and IV HDAC complexes; however, more selective and/or potent agents have been developed (32). We therefore evaluated the effects of several structurally distinct HDAC inhibitors: panobinostat, entinostat, nexturastat A and romidepsin. Panobinostat is also a broad HDAC inhibitor but is more potent than vorinostat (33). As such, panobinostat potently killed MPNSTs when combined with an mTOR inhibitor, and did so at much lower concentrations than vorinostat (20nM versus 2μM) (Fig. 1H versus 1B). Romidepsin, a structurally unrelated compound that inhibits Class I HDAC complexes, but not Class II or IV, was also effective in this context (Fig. 1I). However, more selective HDAC inhibitors such as nexturastat A and entinostat, which suppress HDAC6 and only a subset of Class I HDACs, respectively (34,35), did not kill cells when combined with mTOR inhibitors (Supplementary Fig. S3A and B), suggesting that the broad inhibition of Class I HDAC complexes is required for cell death when combined with mTOR inhibitors.

We therefore replaced vorinostat with panobinostat, and rapamycin with the mTOR kinase inhibitor, sapanisertib for *in vivo* analysis. These agents also promoted dramatic tumor regression *in vivo*, ranging from 45% percent to undetectable in one instance, further supporting the conclusion that mTOR and HDAC inhibitors represent a promising therapeutic combination for these malignancies (Fig. 1J and Supplementary Figure S2B). The observation that rapamycin is effective *in vivo*, mechanistically demonstrates that mTORC1 suppression is sufficient for mediating these effects; however, it remains to be formally established whether rapalogues or mTOR kinase inhibitors will more effectively

inhibit mTORC1 at tolerable doses in humans. Nevertheless, given the substantially higher potency of panobinostat, we believe that the superior efficacy of panobinostat/sapanisertib observed here was largely due to the activity of panobinostat. This conclusion is supported by *in vitro* observations showing that panobinostat induces more cell death than vorinostat when combined with a constant dose of sapanisertib, and does so at 1% of the concentration of vorinostat (Fig. 1B versus 1H).

Oxidative stress precedes and is required for cell death triggered by HDAC and mTOR inhibitors

Our initial hypothesis was that HDAC and mTOR inhibitors might function by triggering catastrophic oxidative stress in these malignancies. To determine whether enhanced oxidative stress was preceding and possibly contributing to the cytotoxic effects of HDAC/mTOR inhibition, expression profiles of MPNSTs were examined 24 hours after treatment, prior to robust cell death observed at 72 hours. Notably, multiple gene sets associated with oxidative stress and ER stress, a tightly linked stress response triggered by ROS-induced protein misfolding, were among the gene sets that were differentially expressed in the HDAC/mTOR inhibitor treated cells (Fig. 2A, Supplementary Table S1). Signatures related to senescence, aging, and hypoxia, additional processes linked to oxidative stress, were also among the recurrent, differentially expressed signatures.

We then investigated whether mTOR inhibitors and HDAC inhibitors were cooperatively enhancing ROS levels in MPNSTs. While HDAC inhibition alone increased ROS, mTOR and HDAC inhibitors together triggered a significantly greater, sustained increase, raising levels by 120% in MPNST cell lines (Fig. 2B (90-8TL, $p=0.001$) and Supplementary Figure S4 (S462, $p=0.007$)). By contrast, in normal cells, in which these agents were unable to trigger cell death (Fig. 1D), ROS induction was substantially lower (Fig. 2B, $p=0.000009$). Most importantly, when MPNSTs were co-treated with n-acetyl cysteine (NAC), a broad-spectrum ROS scavenger, the cooperative effect of sapanisertib and vorinostat on cell death was abolished, demonstrating that the increase in ROS is required for the observed cytotoxicity (Fig. 2C; $p=0.009$). It should be noted that NAC had no effect on target inhibition (Fig. 2D), and also did not disrupt the individual effects of mTOR and HDAC inhibitors on cell proliferation (Fig. 2C), suggesting that oxidative stress does not mediate the cytostatic effects of these agents individually, but is required for the unique, cooperative response that triggers cell death. Finally, we looked for signs of severe oxidative and ER stress *in vivo*. Indeed, electron microscopic analysis of tumors exposed to combined HDAC and mTOR inhibitors *in vivo* revealed severe mitochondrial damage and massive swelling of the endoplasmic reticulum after only 7 hours of treatment (Fig. 2E). Together these observations suggest that severe oxidative stress precedes cell death and is required for the observed cytotoxicity of this combination in these malignancies.

mTOR inhibitors contribute to the therapeutic response by suppressing G6PD and GSH

Previous studies have shown that mTOR inhibitors affect oxidative stress, in part, by suppressing the expression of G6PD and consequently inhibiting the production of reduced glutathione (GSH) (18), one of three major cellular anti-oxidant systems. To investigate whether sapanisertib was indeed functioning through the G6PD/GSH pathway, sapansertib

was replaced by buthionine sulfoximine (BSO), which inhibits glutathione production through a different mechanism (36). Importantly, BSO phenocopied sapanesertib: specifically, BSO exerted modest cytostatic effects as a single agent, but potently killed MPNSTs when combined with HDAC inhibitors *in vitro* (Fig. 2F). Moreover, when administered to tumor bearing animals, BSO alone did not promote tumor regression, but did so when combined with panobinostat, albeit slightly less well than sapanesertib and panobinostat as might be expected (Fig. 2G). Conversely, G6PD overexpression prevented cell death triggered by mTOR and HDAC inhibitors (Fig. 2H). Thus both gain and loss-of function experiments, corroborated by *in vivo* observations, further support the conclusion that cell death is mediated by excessive oxidative stress and that mTOR inhibitors function, in part, by suppressing G6PD and GSH.

HDAC and mTOR Inhibitors cooperate by converging on the Thioredoxin Interacting Protein (TXNIP) and activating Apoptosis Signal-regulating kinase 1 (ASK1)

To deconstruct the molecular mechanism by which these agents cooperatively induce catastrophic oxidative stress and cell death, we examined the transcriptional profiles of cells exposed to combined mTOR and HDAC inhibitors and identified genes that were differentially expressed in response to the combination relative to other treatment groups. Notably, one of the most significantly upregulated genes was thioredoxin interacting protein (*TXNIP*, p=0.0000807). *TXNIP* mRNA expression was modestly elevated in response to sapanisertib and vorinostat alone, but its expression was substantially enhanced by the combination (Fig. 3A). Interestingly, the TXNIP protein binds and inhibits thioredoxin (TRX), a second major cellular anti-oxidant (37). Moreover, the TRX/TXNIP system plays a major role in regulation of redox homeostasis and TXNIP has been shown to mediate cell death caused by oxidative stress in some settings (38,39). The cooperative effects of mTOR and HDAC inhibitors on TXNIP protein levels in MPNST cell lines (S462 and 90-8TLs) was confirmed and quantified by Western analysis, which demonstrated a 10-90-fold increase in protein expression (Fig. 3B–D). TXNIP expression was induced by both vorinostat/sapanisertib (Fig. 3B and C) as well as panobinostat/sapanisertib (Fig. 3D). Notably, the potential involvement of TRX/TXNIP in this therapeutic setting raised the intriguing possibility that the mTOR/HDAC inhibitor combination might be disengaging two of the three major oxidant pathways in MPNSTs: the glutathione and thioredoxin pathways.

To determine whether TXNIP was required for the therapeutic effects of combined HDAC/mTOR inhibition, the *TXNIP* gene was genetically ablated using the CRISPR/Cas9 system. Two CRISPR guide sequences were utilized which both suppressed TXNIP protein induction in drug treated cells (Fig. 3E). Notably, both *sgTXNIP-1* and *sgTXNIP-2* suppressed cell death induced by HDAC and mTOR inhibitors (Fig. 3F and G). Effective *TXNIP* suppression prevented cell death triggered by either vorinostat or panobinostat-based combinations and did so in both S462 (Fig. 3F and G) and 908TLs (Supplementary Figure S5A and B), demonstrating that TXNIP upregulation is essential for the therapeutic effects of this combination.

To complement these loss-of-function studies we evaluated the effects of auranofin, which inhibits thioredoxin through a different mechanism, specifically by suppressing thioredoxin

reductase (40). If mTOR and HDAC inhibitors kill cells by concomitantly suppressing GSH and thioredoxin, then auranofin should be sufficient to functionally replace HDAC inhibitors in this setting. Importantly, auranofin potently cooperated with sapanisertib and triggered MPNST cell death (Fig. 3H). Together with the genetic *TXNIP* ablation studies, these findings confirm the importance of the TXNIP/thioredoxin pathway in this therapeutic response.

In addition to inhibiting the anti-oxidant function of thioredoxin directly, TXNIP specifically induces oxidative stress-induced cell death by triggering the dissociation of Apoptosis Signal-regulating kinase 1(ASK1) from thioredoxin, resulting in its activation (39,41). Importantly, we found that combined mTOR/HDAC inhibitors activated ASK1, as demonstrated by the increased phosphorylation of its downstream target, p38, in both MPNST cell lines in response to either vorinostat or panobinostat-based combinations (Fig. 3I and J). However, to confirm a functional role for ASK1 in cell death, ASK1 expression was ablated using pooled siRNAs targeting the gene that encodes ASK1, *MAP3K5*, in S462 and 90-8TL cells. Similar to the effects of TXNIP ablation, both ASK1-deficient MPNST cell lines were protected from cell death (Fig. 3K and Supplementary Figure S5C, 90-8TL $p<0.0000001$, S462 $p=0.004$). These findings demonstrate that ASK1 activation is essential for cell death triggered by combined HDAC and mTOR inhibitors.

Finally, while these observations suggest that ASK1 mediates the cytotoxic effects of TXNIP, TXNIP has also been shown to inhibit the expression and membrane localization of the glucose transporter, GLUT1 (42). To investigate a potential role for GLUT1 suppression in this response, we ablated the expression of the GLUT1 gene, *SLC2A1*, and determined whether its loss might cooperate with either agent alone or enhance the cytotoxic effects of the combination. GLUT1 suppression did not promote cell death on its own, did not trigger cell death when combined with either agent individually, and if anything slightly ameliorated the cytotoxicity of the combination (Fig. 3L and Supplementary Figure S5D). Taken together these observations suggest that cell death in this setting is primarily mediated through TXNIPs effects on ASK1 activation, rather than GLUT1 suppression.

TXNIP expression is induced through cooperative effects on chromatin and transcription

In other settings HDAC inhibitors have been shown to enhance *TXNIP* expression through direct effects on histone H4 acetylation near the *TXNIP* transcription start site (43), consistent with the modest increase in expression we observe in response to HDAC inhibitors alone (Fig. 3A–D). Accordingly, we found that treatment with vorinostat increased acetylation of histone H4 near the transcriptional start site of *TXNIP* in MPNSTs (Fig. 4A). However, given the cooperative effects of mTOR and HDAC inhibitors, we sought to determine how mTOR inhibitors were contributing to *TXNIP* upregulation. Interestingly, mTOR has been shown to negatively regulate MondoA, a basic helix-loop helix leucine zipper transcription factor that functions in an obligate heterodimer with Mlx. The MondoA-Mlx interaction is suppressed by mTOR activation (44), and is one of two transcriptional complexes known to regulate *TXNIP* expression (43,45). To determine whether MondoA-Mlx was regulating *TXNIP* transcription in this therapeutic context, MondoA expression was ablated using pooled siRNAs that target the gene that encodes MondoA, *MLXIP* (Fig.

4B). MondoA ablation potently inhibited *TXNIP* mRNA (Fig. 4C) and protein expression (Fig. 4D), indicating that the MondoA-Mlx complex is the primary transcriptional regulator of *TXNIP* in this therapeutic setting. Together these findings explain the observed cooperativity between HDAC and mTOR inhibitors, which respectively open chromatin at the *TXNIP* promoter and induce *TXNIP* transcription through activation of the MondoA-Mxl complex.

Combined HDAC and mTOR inhibitors kill NF1- and KRAS- mutant lung cancers

Finally, to determine whether this combination might be effective in other Ras-pathway driven tumors we evaluated these agents in non-small cell lung cancer cell (NSCLC) lines that harbored either *NF1* or *KRAS* mutations, as *NF1* and *KRAS* mutations occur in 11% and 33% percent of human NSCLC, respectively (46). Notably, the HDAC/mTOR inhibitor combination killed both *NF1*-deficient NSCLC lines and 2 out of 3 *KRAS* mutant lines (Fig. 4E). Moreover, similar to findings in the autochthonous MPNST model, combined HDAC/mTOR inhibitors triggered robust tumor regression *in vivo* in a xenograft model of *KRAS*-mutant NSCLC (Fig. 4F and G). These observations suggest that utility of this combination may extend beyond nervous system malignancies, and represents a promising therapeutic approach for at least a subset of *NF1* and *KRAS* mutant lung cancers for which there are currently no effective treatments.

Discussion

The ability to identify and inhibit specific oncogenic drivers in cancer has changed the standard of care for many diseases (1). Nevertheless, relatively few tumor types harbor single, targetable driving alterations and even those that do often acquire resistance to such therapies. These observations suggest that additional therapeutic strategies are needed. One approach may be to concomitantly target key oncogenic pathways along with other cancer-specific vulnerabilities. However, the challenge has been to both identify critical dependencies in a given tumor type, as well as selectively target these vulnerabilities while sparing normal tissue.

Chronic oxidative stress has been proposed to represent a potential cancer-specific vulnerability (2,4). Indeed, the excessive production of ROS in already sensitized tumor cells is thought to contribute to the efficacy of some chemotherapies (7,8). However, given the general toxicity of these agents, a more targeted approach, designed to selectively induce oxidative stress in tumors, is needed. Here we identify a promising drug combination that functions by triggering irresolvable, catastrophic oxidative stress in *NF1*-mutant malignancies *in vitro* and *in vivo* (Fig. 5). Specifically, we show that mTOR and HDAC inhibitors suppress thioredoxin, a major anti-oxidant, by potently inducing the expression of its direct inhibitor, TXNIP, through cooperative effects on chromatin and transcription. Importantly, cell death is preceded and mediated by excessive oxidative stress as well as ASK1 activation, an apoptotic kinase normally suppressed by thioredoxin. Notably, mTOR inhibitors have previously been shown to suppress another anti-oxidant, GSH; however, mTOR inhibitors are not sufficient to induce irresolvable oxidative stress or cell death. Here we show that the HDAC/mTORi combination is effective because it inhibits a second major

anti-oxidant pathway in these cancers. As such, two of the three major anti-oxidant pathways are suppressed by this combination. Importantly, while the HDAC/mTOR inhibitor combination kills *NF1*-mutant nervous system malignancies as well as *NF1* and *KRAS* mutant lung cancers, it does not kill normal cells and it is not toxic to mice *in vivo*.

While the majority of this study has focused on MPNSTs, the therapeutic effect of these agents in *KRAS* and *NF1*-mutant lung cancer is striking and warrants further investigation. MPNSTs that arise in individuals with NF1 are inherently more homogeneous as compared to lung cancer, in that they are initiated by *NF1* mutations and progress due to a specific set of additional genetic alterations (47–49). In contrast, lung cancers are much more genetically and biologically heterogeneous (50,51). While 4/5 of the RAS pathway-driven lung cancers evaluated in this study were sensitive to these agents, further study is needed to establish whether *NF1* and *KRAS* mutations are predictive biomarkers, and/or if other predictive biomarkers exist. Sensitivity to this combination may ultimately be dictated by the specific anti-oxidant pathways that are upregulated in a given tumor, and whether or not mTOR and HDACs serve as critical buffering pathways. Nevertheless, given that there are currently no effective therapies for both *NF1* and *RAS* mutant lung cancers, these findings reveal a potential therapeutic strategy that can be further investigated.

Currently, there are no effective treatments for any *NF1* or *KRAS* mutant cancers. Moreover, while promising agents designed to target a subset of mutant KRAS proteins are being developed (52,53), even if successful, durable regressions are likely to require a drug combination rather than a single agent. These studies demonstrate that enhanced oxidative stress represents a tractable vulnerability in these RAS-driven tumors: a finding that can be used to inspire clinical trials now and in the context of future combinations. Fortunately, HDAC inhibitors and rapalogues are currently being evaluated in the clinic for other indications, based on an unrelated mechanistic rationale (clinicaltrials.gov). Therefore tolerable doses of relevant drug combinations have been established (31,54) and doses of additional combinations will become available in the near future (NCT00918333, NCT01341834). Nevertheless, efficacy in solid tumors may require the most potent and/or specific agents. Our data support the evaluation of combinations using either potent pan-HDAC (e.g. panobinostat) or Class I-specific HDAC inhibitors and suggest that selective HDAC 1/3 or HDAC 6 inhibitors will not be effective in these tumors. Regardless, these studies have identified a promising new therapeutic combination for these currently untreatable tumors and demonstrate that approaches to selectively enhance oxidative stress in cancer cells may be more broadly exploited for the development of effective combination therapies.

Methods

Cell Lines and Reagents

SNF96.2 (2009), S462 (2003), H1435 (2014), H1838 (2014), H1573 and IMR-90 (2011) were purchased from the ATCC in the year indicated. H23 and H1792 were generously provided by Dr. Pasi Janne (Dana Farber Cancer Institute, Boston, MA) in 2008. 90-8TL was generously provided by Dr. Eric Legius (KU Leuven, Belgium) in 2002. 88-14 was generously provided by Dr. Jonathan Fletcher (Dana Farber Cancer Institute, Boston, MA)

in 2012. T265 was generously provided by Dr. Eduard Serra (Institut de Medicina Predictiva i Personalitzada del Càncer, Barcelona, Spain) in 2016. No further authentication of these cell lines was performed. 90-8TL and S462 were tested for mycoplasma in March 2013 (negative). The other cell lines in this study have not been tested for mycoplasma. Cells were used for experiments in the paper within 15-20 passages from thawing, with the exception of IMR-90, which were used within 10 passages. H23, H1435, S462, 88-14, T265, SNF96.2 and 90-8TL were cultured in DMEM supplemented with fetal bovine serum (10%) and L-glutamine. H1792, H1838, and H1573 were cultured in RPMI supplemented with fetal bovine serum (10%) and L-glutamine. IMR-90s were cultured in MEM supplemented with fetal bovine serum (10%) and L-glutamine. Cells were grown in normoxic conditions, and all experiments were performed in normoxic conditions. Antibodies were obtained from the following sources: Cell Signaling Technologies: $pS6^{S235/236}$ (2211), S6 (2217), TXNIP (14715), Vinculin (4650), $pP38^{T180/Y182}$ (9211), P38 (9212), ASK1 (8662), Glut1 (12939); Sigma Aldrich: Actin (A2066), Tubulin (T5168); EMD Millipore: Acetylated H3K9 (06-942), Bethyl: G6PD (A300-404A). Sapanisertib, Nexturastat A, romidepsin, panobinostat (*in vitro*), entinostat, and vorinostat were purchased from Selleck Chemicals. Rapamycin and panobinostat (*in vivo*) were purchased from LC Labs. Auranofin was purchased from Santa Cruz Biotechnologies. Buthionine Sulfoximine was purchased from Sigma Aldrich. Carboxy-H2DCFDA was purchased from Life Technologies (#C400).

RNAi

Non-targeting, *HDAC1, HDAC2, HDAC3, HDAC6, MLXIP, MAP3K5*, and *SLC2A1* siRNA pools were purchased from GE Healthcare/Dharmacon (D-001810-10, L-003493-00, L-003495-02, L-003496-00, L-003499-00, L-008976-00, L-003584-00, and L-007509-02, respectively). siRNAs were transfected overnight using RNAiMax lipofectamine from Invitrogen.

CRISPR

CRSIPR guides targeting *LACZ* (GCTGGAGTGCGATCTTCCTG), and TXNIP (sg-*TXNIP*-1: GGGACATGCGCATCATGGCG, sg*TXNIP*-2: CAGAAGTTGTCATCAGTCAG) were generated and cloned into lentiCRISPRv2 by Dr. Gerald Marsischky at the Genome Engineering Production Group (GEPG) at Harvard Medical School.

Chromatin Immunoprecipitation (ChIP)

90-8TLs were treated with vehicle or vorinostat for 6 hours and then cross-linked for 10 minutes with an 11% formaldehyde solution, and cell lysis was performed according to the Agilent mammalian ChIP-on-Chip protocol. Lysates were sonicated on ice for 45 minutes, 20 seconds on, 40 seconds off, in a Misonix Cup Horn Sonicator at 4˚C. Chromatin was immunoprecipitated overnight at 4˚C with acetylated histone H4 antibody (Active Motif) or rabbit IgG (Millipore), which had first been conjugated to protein G magnetic beads (Life Technologies 10004D).

Quantitative PCR

RNA was extracted from cells after indicated treatments using Trizol (Invitrogen). Primers for *TXNIP* (gene expression) have been previously described (55) and ordered from Invitrogen. Primers for *MLXIP* were (5′−3′): GCCAACAGGTGAGAATGAGA (Forward) and TTCCTTTGAAGGATGTTCCC (Reverse). Primers for *MAP3K5* were (5′−3′): AGACATCTGGTCTCTGGGC (Forward) and AACATTCCCACCTTGAACAT (Reverse). All samples were normalized to human HPRT1. Primers for HPRT1 were (5′−3′) GCCGGCTCCGTTATGG (Forward) and AACCTGGTTCATCATCACTA (Reverse). ChIP-PCR primers for *TXNIP* were (5′−3′): CAAGCATTCCTTATCACACAGATG (Forward) and GTGATCAAAGGAGGGCAAGATA (Reverse). ChIP-PCR primers for *GAPDH* have been previously published (43). Quantitative Real-Time PCR was performed using qScript SYBR green.

Cell Growth Studies

Approximately 175,000 per well were seeded into 6-well plates. For siRNA experiments, cells were seeded 12 to 16 hours after transfection. Twenty-four hours after plating, day 0 counts were taken using a hemocytometer. For inhibitor experiments, drug treatments were started at this time. Final cell counts were taken 72 hours after day 0 counts. Unless otherwise indicated, drug concentrations were as follows: vorinostat (2μM), romidepsin (1nM), panobinostat (20nM), sapanisertib (200nM for all cell lines except 90-8TLs, where sapanisertib was used at 100nM), auranofin (750nM), buthionine sulfoximine (200 μM). The concentration of sapanisertib (200nM) was chosen based on previously published studies (23,56,57). 100nM was used in 90-8TLs for historical reasons but 200nM produces the same results. We confirmed that this concentration of sapanisertib effectively inhibited mTOR in all instances and induced a maximal cytostatic response as a single agent. The concentration of Vorinostat was selected based on previous studies which typically use 1-5μM (58). 2μM was selected because this concentration effectively inhibited histone deacetylation and exerted minimal effects on cell viability on its own. Dose response curves were initially performed to identify concentrations of panobinostat and romidepsin. Final concentrations were selected that effectively inhibited histone deacetylation and induced minimal or no cell death as single agents. For agents that did not have an effect (Nexturastat A, Entinostat) a range of concentrations are shown to demonstrate that these are indeed inactive even at the highest concentrations.

In Vivo Drug Treatments

Animal procedures were approved by the Center for Animal and Comparative Medicine in Harvard Medical School in accordance with the NIH Guide for the Care and Use of Laboratory Animals and the Animal Welfare Act (Protocol #03379). C56/BL6 NPcis mice have been previously described (27). A power analysis was used to determine the number of mice per treatment group. Both male and female mice were used. Mice were treated daily with rapamycin via i.p. injection at 5 mg/kg, which was prepared as previously described (16). Vorinostat was administered at 50 mg/kg once daily via i.p. injection. Vorinostat was dissolved directly into (2-Hydroxypropyl)-β-cyclodextrin (Sigma Aldrich C0926). Panobinostat was administered via i.p. injection at 10mg/kg once daily. Panobinostat was

dissolved into DMSO, and then diluted into 10% (2-hydroxypropyl)- beta-cyclodextrin. Sapanisertib was prepared in a solution of 5% N-methyl- 2-pyrrolidone and 15% polyvinylpyrrolidone, and administered via oral gavage once daily at 0.8mg/kg. Buthionine Sulfoximine was dissolved directly into the drinking water and administered at 20mM.

Tumor Volume Measurements

Treatment was initiated when tumors reached approximately 200–700mm^3. Tumor measurements were taken using a vernier caliper. Tumor volume was calculated using the standard formula: $L \times W^2 \times 0.52$.

Microarray and Analysis

RNA was isolated from 90-8TL cells 24 hours after treatment with indicated drugs. RNA was isolated using Trizol, following the manufacturer's protocol, and RNA cleanup was performed using the Qiagen RNeasy kit (#74104). The Molecular Biology Core Facilities at Dana-Farber Cancer Institute hybridized RNA to the Affymetrix Human 1.0 STS array chip. To determine genes and gene sets differentially expressed amongst treatment groups a class comparison analysis was performed using BRB-Array tools developed by Dr. Richard Simon (National Cancer Institute, NIH, Rockville, MD) and the BRB ArrayTools Development team. Microarray data can be accessed in the GEO database (accession number GSE84205).

DCFDA staining

Cells were treated as indicated. Cells were then stained with H2DCFDA at 10μM and analyzed by flow cytometry.

Electron Microscopy

Tumor samples were collected 7 hours after a single treatment with 5mg/kg rapamycin and 100mg/kg vorinostat. Tissue was cut into 1mM cubes and fixed in 2% glutaraldehyde and 4% paraformaldehyde in 0.1M sodium cacodylate buffer, and then processed by the Electron Microscopy Facility at the University of Chicago as previously described (59). Images were collected and analyzed by Dr. Kay Macleod (University of Chicago).

Xenograft Model

For xenograft study, 2.5 million H1573 cells in 50% matrigel were injected into the flanks of female nude mice, and tumors were allowed to form. When tumors were between 130mm^3 and 350mm^3 animals were assigned to a treatment group. Tumors were measured every 2-3 days with a vernier caliper. Body condition and weight loss were monitored as signs of toxicity.

Statistics

Quantitative measurements are graphed as mean ± standard deviation (SD) of three technical replicates, unless otherwise indicated. To determine significance, an ANOVA analysis was performed, followed by either a 2-tailed unpaired *t* test or Bonferonni's multiple comparison test when multiple groups were considered. For quantitative experiments, a p-value of less

than 0.05 was considered significant, and p-values are shown when statistical tests were used. For microarray analysis (class comparison analysis of genes and gene sets) lower significance thresholds were used (unadjusted $p<0.001$ and unadjusted $p<0.005$, respectively) to narrow the focus to the genes and pathways most significantly impacted by the combination treatment. P-values shown are adjusted for multiple hypothesis testing when applicable, unless otherwise noted. All data was graphed and analyzed using Prism 7, with the exception of the microarray data which was analyzed using BRB-Array tools.

Supplementary Material

Refer to Web version on PubMed Central for supplementary material.

Acknowledgments

This work was supported by grants from the Children's Tumor Foundation and the NCI (5R01CA111754-08). CM was supported by a Young Investigator Award from the Children's Tumor Foundation. OM was supported, in part, by a Latsis fellowship. We would like to thank Yiling Qiu at the Partners Flow Cytometry Core for his technical assistance. We would also like to acknowledge the Molecular Biology Core Facility at Dana Farber Cancer Institute for performing the microarray analysis.

Financial Support: This work was supported by grants from the NCI (R01 R01CA111754, K.C.) and the Children's Tumor Foundation (CM and KC).

References

1. Neal, JW., Sledge, GW. Nature Reviews Clinical Oncology. Vol. 11. Nature Publishing Group; 2014. Decade in review[mdash]targeted therapy: Successes, toxicities and challenges in solid tumours; p. 627-8.
2. Luo J, Solimini NL, Elledge SJ. Principles of cancer therapy: oncogene and non-oncogene addiction. Cell. 2009; 136:823–37. [PubMed: 19269363]
3. Trachootham, D., Lu, W., Ogasawara, MA., Valle, NR-D., Huang, P. Redox Regulation of Cell Survival. Vol. 10. Mary Ann Liebert, Inc; 140 Huguenot Street, 3rd Floor New Rochelle, NY 10801 USA: 2010. p. 1343-74.http://dxdoiorg/101089/ars20071957
4. Gorrini C, Harris IS, Mak TW. Modulation of oxidative stress as an anticancer strategy. Nat Rev Drug Discov. 2013; 12:931–47. [PubMed: 24287781]
5. Harris IS, Treloar AE, Inoue S, Sasaki M, Gorrini C, Lee KC, et al. Glutathione and thioredoxin antioxidant pathways synergize to drive cancer initiation and progression. Cancer Cell. 2015; 27:211–22. [PubMed: 25620030]
6. DeNicola GM, Karreth FA, Humpton TJ, Gopinathan A, Wei C, Frese K, et al. Oncogene-induced Nrf2 transcription promotes ROS detoxification and tumorigenesis. Nature. 2011; 475:106–9. [PubMed: 21734707]
7. Conklin KA. Chemotherapy-associated oxidative stress: impact on chemotherapeutic effectiveness. Integr Cancer Ther SAGE Publications. 2004; 3:294–300.
8. Barrera, G., Barrera, G. International Scholarly Research Notices. Vol. 2012. Hindawi Publishing Corporation; 2012. Oxidative Stress and Lipid Peroxidation Products in Cancer Progression and Therapy; p. 1-21.
9. Ding L, Getz G, Wheeler DA, Mardis ER, McLellan MD, Cibulskis K, et al. Somatic mutations affect key pathways in lung adenocarcinoma. Nature. 2008; 455:1069–75. [PubMed: 18948947]
10. Maertens O, Johnson B, Hollstein P, Frederick DT, Cooper ZA, Messiaen L, et al. Elucidating distinct roles for NF1 in melanomagenesis. Cancer Discov. 2013; 3:338–49. [PubMed: 23171796]
11. McGillicuddy LT, Fromm JA, Hollstein PE, Kubek S, Beroukhim R, De Raedt T, et al. Proteasomal and genetic inactivation of the NF1 tumor suppressor in gliomagenesis. Cancer Cell. 2009; 16:44–54. [PubMed: 19573811]

12. Parsons DW, Jones S, Zhang X, Lin JC-H, Leary RJ, Angenendt P, et al. An integrated genomic analysis of human glioblastoma multiforme. Science. 2008; 321:1807–12. [PubMed: 18772396]
13. Ratner N, Miller SJ. A RASopathy gene commonly mutated in cancer: the neurofibromatosis type 1 tumour suppressor. Nat Rev Cancer. 2015; 15:290–301. [PubMed: 25877329]
14. Maertens O, Cichowski K. An expanding role for RAS GTPase activating proteins (RAS GAPs) in cancer. Adv Biol Regul. 2014; 55:1–14. [PubMed: 24814062]
15. Zehou O, Fabre E, Zelek L, Sbidian E, Ortonne N, Banu E, et al. Chemotherapy for the treatment of malignant peripheral nerve sheath tumors in neurofibromatosis 1: a 10-year institutional review. Orphanet J Rare Dis. 2013; 8:127. [PubMed: 23972085]
16. Johannessen CM, Johnson BW, Williams SMG, Chan AW, Reczek EE, Lynch RC, et al. TORC1 is essential for NF1-associated malignancies. Curr Biol. 2008; 18:56–62. [PubMed: 18164202]
17. Düvel K, Yecies JL, Menon S, Raman P, Lipovsky AI, Souza AL, et al. Activation of a metabolic gene regulatory network downstream of mTOR complex 1. Mol Cell. 2010; 39:171–83. [PubMed: 20670887]
18. De Raedt T, Walton Z, Yecies JL, Li D, Chen Y, Malone CF, et al. Exploiting cancer cell vulnerabilities to develop a combination therapy for ras-driven tumors. Cancer Cell. 2011; 20:400–13. [PubMed: 21907929]
19. Malone CF, Fromm JA, Maertens O, DeRaedt T, Ingraham R, Cichowski K. Defining Key Signaling Nodes and Therapeutic Biomarkers in NF1-Mutant Cancers. Cancer Discov American Association for Cancer Research. 2014; 4:1062–73.
20. Petruccelli LA, Dupéré-Richer D, Pettersson F, Retrouvey H, Skoulikas S, Miller WH. Vorinostat induces reactive oxygen species and DNA damage in acute myeloid leukemia cells. PLoS ONE. 2011; 6:e20987. [PubMed: 21695163]
21. Choo AY, Yoon S-O, Kim SG, Roux PP, Blenis J. Rapamycin differentially inhibits S6Ks and 4E-BP1 to mediate cell-type-specific repression of mRNA translation. Proc Natl Acad Sci USA. 2008; 105:17414–9. [PubMed: 18955708]
22. Choo AY, Blenis J. Not all substrates are treated equally: implications for mTOR, rapamycin-resistance and cancer therapy. Cell Cycle. 2009; 8:567–72. [PubMed: 19197153]
23. Lock R, Ingraham R, Maertens O, Miller AL, Weledji N, Legius E, et al. Cotargeting MNK and MEK kinases induces the regression of NF1-mutant cancers. J Clin Invest American Society for Clinical Investigation. 2016; 126:2181–90.
24. Foucquier J, Guedj M. Analysis of drug combinations: current methodological landscape. Pharmacol Res Perspect. 2015; 3:e00149. [PubMed: 26171228]
25. Yang H, Higgins B, Kolinsky K, Packman K, Go Z, Iyer R, et al. RG7204 (PLX4032), a selective BRAFV600E inhibitor, displays potent antitumor activity in preclinical melanoma models. Cancer Res American Association for Cancer Research. 2010; 70:5518–27.
26. Ji H, Li D, Chen L, Shimamura T, Kobayashi S, McNamara K, et al. The impact of human EGFR kinase domain mutations on lung tumorigenesis and in vivo sensitivity to EGFR-targeted therapies. Cancer Cell. 2006; 9:485–95. [PubMed: 16730237]
27. Cichowski K, Shih TS, Schmitt E, Santiago S, Reilly K, McLaughlin ME, et al. Mouse models of tumor development in neurofibromatosis type 1. Science. 1999; 286:2172–6. [PubMed: 10591652]
28. Stemmer-Rachamimov AO, Louis DN, Nielsen GP, Antonescu CR, Borowsky AD, Bronson RT, et al. Comparative pathology of nerve sheath tumors in mouse models and humans. Cancer Res American Association for Cancer Research. 2004; 64:3718–24.
29. Tabernero J, Rojo F, Calvo E, Burris H, Judson I, Hazell K, et al. Dose- and Schedule-Dependent Inhibition of the Mammalian Target of Rapamycin Pathway With Everolimus: A Phase I Tumor Pharmacodynamic Study in Patients With Advanced Solid Tumors. Journal of Clinical Oncology American Society of Clinical Oncology. 2016; 26:1603–10.
30. Mahalati K, Kahan BD. Clinical pharmacokinetics of sirolimus. Clin Pharmacokinet. 2001; 40:573–85. [PubMed: 11523724]
31. Park H, Garrido-Laguna I, Naing A, Fu S, Falchook GS, Piha-Paul SA, et al. Phase I dose-escalation study of the mTOR inhibitor sirolimus and the HDAC inhibitor vorinostat in patients with advanced malignancy. Oncotarget. 2016; 7

32. Falkenberg KJ, Johnstone RW. Histone deacetylases and their inhibitors in cancer, neurological diseases and immune disorders. Nat Rev Drug Discov Nature Research. 2015; 14:219–9.
33. Anne, M., de Sammartino, D., Barginear, M., Budman, D. OTT. Vol. 6. Dove Press; 2013. Profile of panobinostat and its potential for treatment in solid tumors: an update; p. 1613-24.
34. Bergman JA, Woan K, Perez-Villarroel P, Villagra A, Sotomayor EM, Kozikowski AP. Selective histone deacetylase 6 inhibitors bearing substituted urea linkers inhibit melanoma cell growth. J Med Chem. 2012; 55:9891–9. [PubMed: 23009203]
35. Hu E, Dul E, Sung C-M, Chen Z, Kirkpatrick R, Zhang G-F, et al. Identification of novel isoform-selective inhibitors within class I histone deacetylases. J Pharmacol Exp Ther American Society for Pharmacology and Experimental Therapeutics. 2003; 307:720–8.
36. Griffith OW, Meister A. Potent and specific inhibition of glutathione synthesis by buthionine sulfoximine (S-n-butyl homocysteine sulfoximine). J Biol Chem. 1979; 254:7558–60. [PubMed: 38242]
37. Hwang J, Suh H-W, Jeon YH, Hwang E, Nguyen LT, Yeom J, et al. The structural basis for the negative regulation of thioredoxin by thioredoxin-interacting protein. Nat Commun. 2014; 5:2958. [PubMed: 24389582]
38. Saxena G, Chen J, Shalev A. Intracellular shuttling and mitochondrial function of thioredoxin-interacting protein. J Biol Chem. 2010; 285:3997–4005. [PubMed: 19959470]
39. Lu J, Holmgren A. Thioredoxin system in cell death progression. Antioxid Redox Signal. 2012; 17:1738–47. [PubMed: 22530689]
40. Marzano C, Gandin V, Folda A, Scutari G, Bindoli A, Rigobello MP. Inhibition of thioredoxin reductase by auranofin induces apoptosis in cisplatin-resistant human ovarian cancer cells. Free Radic Biol Med. 2007; 42:872–81. [PubMed: 17320769]
41. Saitoh M, Nishitoh H, Fujii M, Takeda K, Tobiume K, Sawada Y, et al. Mammalian thioredoxin is a direct inhibitor of apoptosis signal-regulating kinase (ASK) 1. EMBO J. 1998; 17:2596–606. [PubMed: 9564042]
42. Wu N, Zheng B, Shaywitz A, Dagon Y, Tower C, Bellinger G, et al. AMPK-Dependent Degradation of TXNIP upon Energy Stress Leads to Enhanced Glucose Uptake via GLUT1. Mol Cell. 2013; 49:1167–75. [PubMed: 23453806]
43. Cha-Molstad H, Saxena G, Chen J, Shalev A. Glucose-stimulated expression of Txnip is mediated by carbohydrate response element-binding protein, p300, and histone H4 acetylation in pancreatic beta cells. J Biol Chem. 2009; 284:16898–905. [PubMed: 19411249]
44. Kaadige MR, Yang J, Wilde BR, Ayer DE. MondoA-Mlx transcriptional activity is limited by mTOR-MondoA interaction. Mol Cell Biol. 2015; 35:101–10. [PubMed: 25332233]
45. Stoltzman CA, Peterson CW, Breen KT, Muoio DM, Billin AN, Ayer DE. Glucose sensing by MondoA:Mlx complexes: a role for hexokinases and direct regulation of thioredoxin-interacting protein expression. Proc Natl Acad Sci USA National Acad Sciences. 2008; 105:6912–7.
46. Cancer Genome Atlas Research Network. Comprehensive molecular profiling of lung adenocarcinoma. Nature. 2014; 511:543–50. [PubMed: 25079552]
47. Kim A, Stewart DR, Reilly KM, Viskochil D, Miettinen MM, Widemann BC. Malignant Peripheral Nerve Sheath Tumors State of the Science: Leveraging Clinical and Biological Insights into Effective Therapies. Sarcoma Hindawi. 2017; 2017:1–10.
48. De Raedt T, Beert E, Pasmant E, Luscan A, Brems H, Ortonne N, et al. PRC2 loss amplifies Ras-driven transcription and confers sensitivity to BRD4-based therapies. Nature. 2014; 514:247–51. [PubMed: 25119042]
49. Lee W, Teckie S, Wiesner T, Ran L, Prieto Granada CN, Lin M, et al. PRC2 is recurrently inactivated through EED or SUZ12 loss in malignant peripheral nerve sheath tumors. Nat Genet. 2014; 46:1227–32. [PubMed: 25240281]
50. Chen Z, Fillmore CM, Hammerman PS, Kim CF, Wong K-K. Non-small-cell lung cancers: a heterogeneous set of diseases. Nat Rev Cancer. 2015; 15:247–7.
51. Redig AJ, Capelletti M, Dahlberg SE, Sholl LM, Mach S, Fontes C, et al. Clinical and Molecular Characteristics of NF1-Mutant Lung Cancer. Clin Cancer Res. 2016; 22:3148–56. [PubMed: 26861459]

52. Ostrem JM, Peters U, Sos ML, Wells JA, Shokat KM. K-Ras(G12C) inhibitors allosterically control GTP affinity and effector interactions. Nature. 2013; 503:548–51. [PubMed: 24256730]

53. Lim SM, Westover KD, Ficarro SB, Harrison RA, Choi HG, Pacold ME, et al. Therapeutic targeting of oncogenic K-Ras by a covalent catalytic site inhibitor. Angew Chem Int Ed Engl. 2014; 53:199–204. [PubMed: 24259466]

54. Zibelman M, Wong Y-N, Devarajan K, Malizzia L, Corrigan A, Olszanski AJ, et al. Phase I study of the mTOR inhibitor ridaforolimus and the HDAC inhibitor vorinostat in advanced renal cell carcinoma and other solid tumors. Invest New Drugs Springer US. 2015; 33:1040–7.

55. Elgort MG, O'Shea JM, Jiang Y, Ayer DE. Transcriptional and Translational Downregulation of Thioredoxin Interacting Protein Is Required for Metabolic Reprogramming during G(1). Genes Cancer. 2010; 1:893–907. [PubMed: 21779470]

56. Zhang X, Ding Z, Mo J, Sang B, Shi Q, Hu J, et al. GOLPH3 promotes glioblastoma cell migration and invasion via the mTOR-YB1 pathway in vitro. Molecular Carcinogenesis. 2015; 54:1252–63. [PubMed: 25156912]

57. Ashouri JF, Weiss A. Endogenous Nur77 Is a Specific Indicator of Antigen Receptor Signaling in Human T and B Cells. J Immunol American Association of Immunologists. 2017; 198:657–68.

58. Sun X, Hasanali ZS, Chen A, Zhang D, Liu X, Wang H-G, et al. Suberoylanilide hydroxamic acid (SAHA) and cladribine synergistically induce apoptosis in NK-LGL leukaemia. Br J Haematol (4). 2015; 168:371–83. [PubMed: 25284154]

59. Barth, S., Glick, D., Macleod, KF. J Pathol. Vol. 221. John Wiley & Sons, Ltd; 2010. Autophagy: assays and artifacts; p. 117-24.

Statement of Significance

There are no effective therapies for *NF1* or *RAS* mutant cancers. We show that combined mTOR/HDAC inhibitors kill these RAS-driven tumors by causing catastrophic oxidative stress. This study identifies a promising therapeutic combination and demonstrates that selective enhancement of oxidative stress may be more broadly exploited for developing cancer therapies.

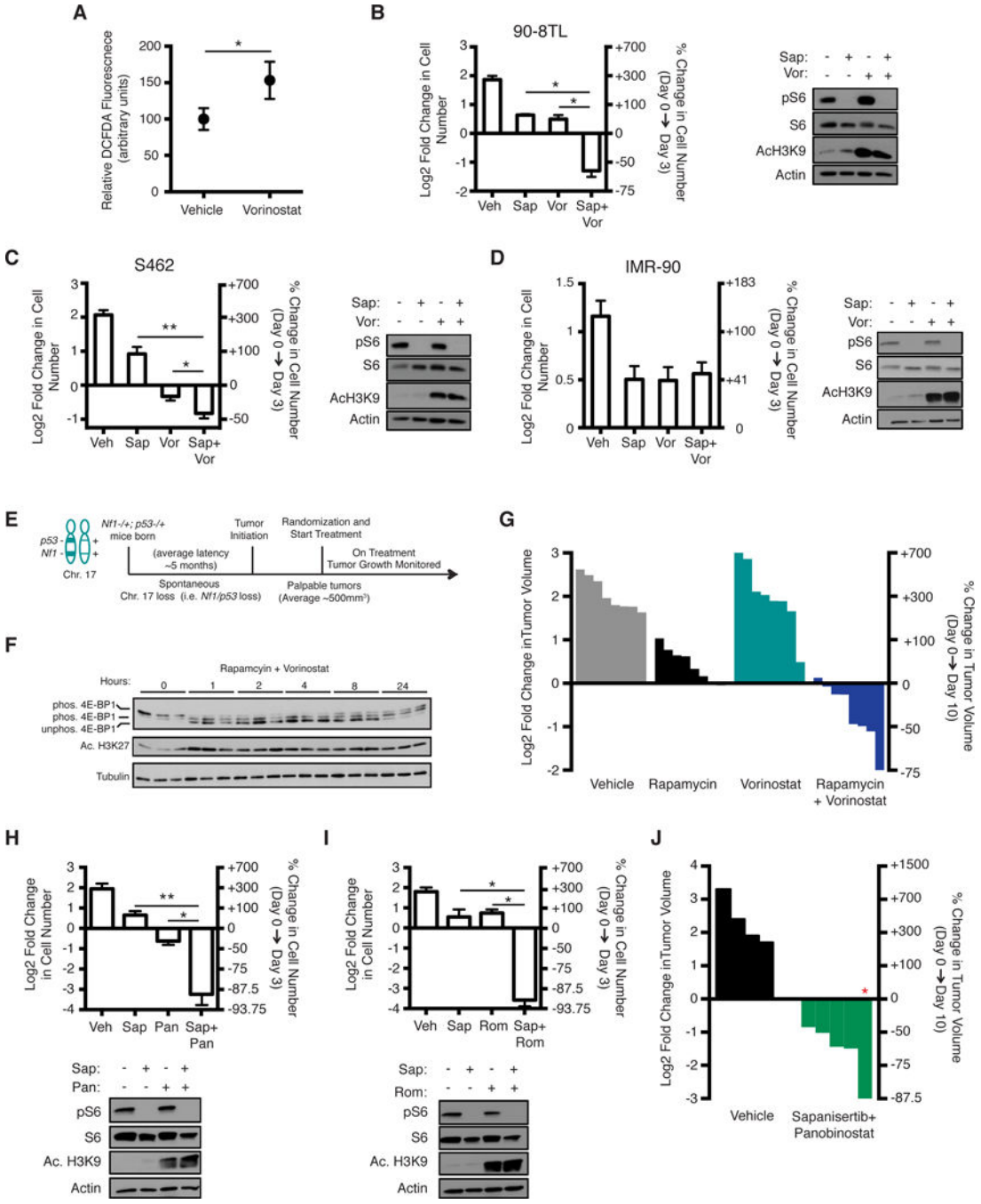

Figure 1. Combined HDAC and mTOR inhibitors kill *NF1*-mutant malignancies *in vitro* and *in vivo*

A) S462 cells treated with either vehicle or vorinostat (2μM) for 24 hours were stained with dichlorofluorescin diacetate (DCFDA), a dye that measures reactive oxygen species (ROS). Graph indicates relative mean DCFDA (arbitrary units, three independent experiments; **p*=0.006, paired two-tailed student t-test). **B)** 90-8TL cells were treated with vehicle, sapanisertib (100nM), vorinostat (2μM), or sapanisertib + vorinostat, for 3 days. Left y-axis indicates log 2 of fold change in cell number at 3 days relative to day 0. Right y-axis

indicates percent change in cell number at 3 days on a log 2 scale. Error bars ±SD from technical triplicates. At right, immunoblot shows levels of phosphorylated S6 (pS6) and histone H3 acetylation at lysine 9 (AcH3K9) after 24 hours of indicated treatment. S6 and Actin serve as controls. *p<0.000001 C) S462 cells were treated with vehicle, sapanisertib (200nM), vorinostat (2μM), or sapanisertib and vorinostat and evaluated as described in B. *p=0.009599, **p=0.000002 D) Non-transformed IMR-90 (lung fibroblast) cells treated and evaluated as described in C. **E)** Schematic of *in vivo* experimental design. **F)** *In vivo* pharmacodynamic analysis showing acetylated histone H3 at lysine 27 (Ac.H3K27) and 4E-BP1 in tissue from animals treated with vorinostat and rapamycin for the indicated amount of time. Lines indicate hyper-phosphorylated and hypo-phosphorylated species of 4E-BP1. Tubulin serves as a control. **G)** Waterfall plot depicting change in tumor volume after 10 days of treatment with single and combined agents as indicated. Each of the four experimental groups of mice were treated as part of the same experiment. The data shown for the vehicle and rapamycin treatments are reproduced from Figure 2 A/C of reference 19. Left y-axis depicts log2 fold change in tumor volume after 10 days. The Log2 values on the left axis have been converted to the actual percent increase or decrease in tumor volume to best appreciate relative changes, shown on the right y-axis. Each bar represents an individual tumor. **H)** 90-8TL cells were treated with vehicle, sapanisertib (100nM), panobinostat (20nM), or sapanisertib and panobinostat and evaluated as described in B. *p=0.000021, **p=0.000001 **I)** 90-8TL cells were treated with romidepsin (1nM), sapanisertib (100nM), or romidepsin + sapanisertib and evaluated as described in B. *p<0.000001 J) Waterfall plot depicting log2 fold change in tumor volume after 10 days of treatment with vehicle or panobinostat + sapanisertib. The Log2 values on the left axis have been converted to the actual percent increase or decrease in tumor volume to best appreciate relative changes, shown on the right y-axis.“ * ” denotes tumor that was undetectable by palpation at 10 days. Tumor size was determined by measuring residual flat lesion/tissue after dissection.

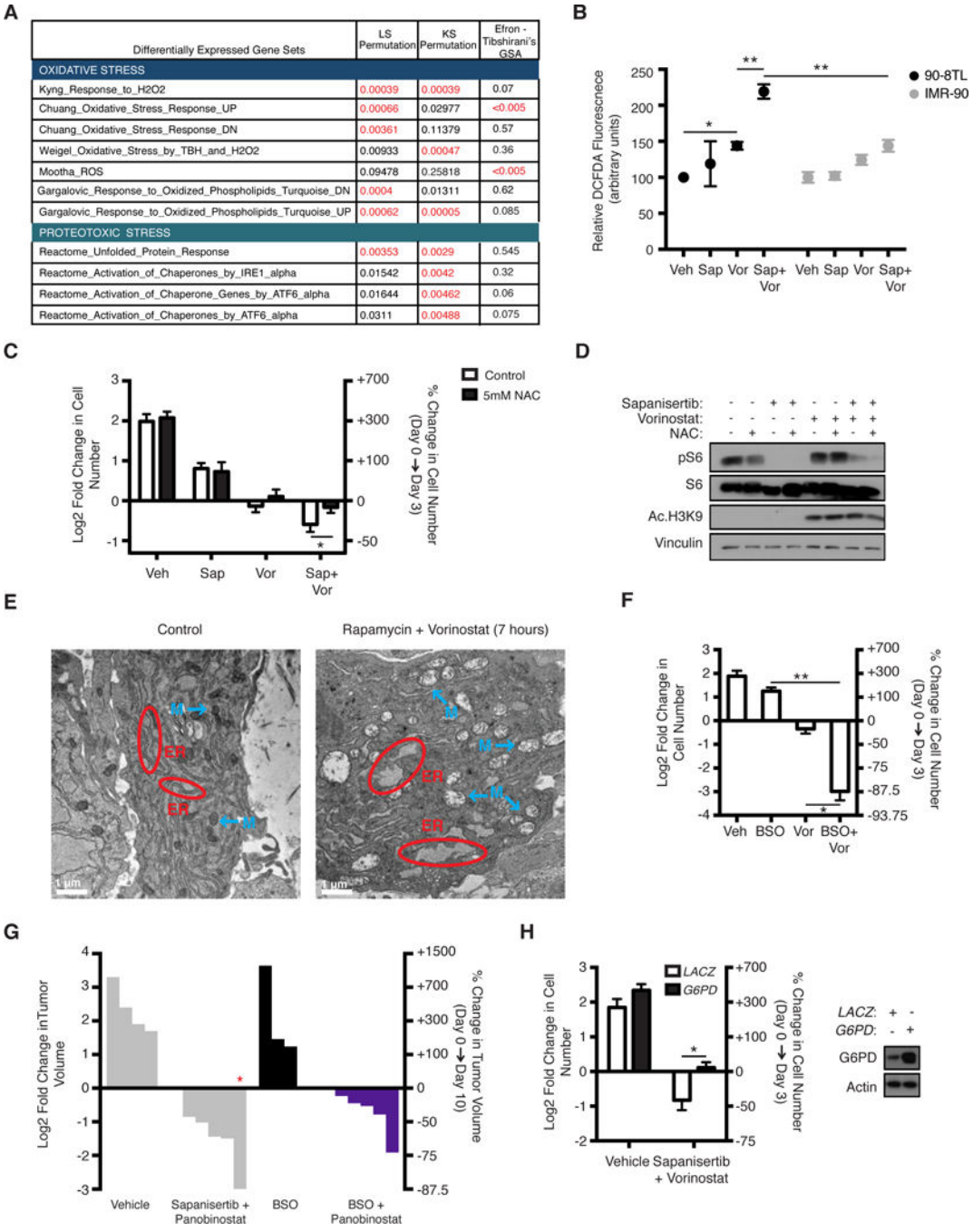

Figure 2. The therapeutic effects of HDAC and mTOR inhibitors are mediated by the suppression of Class I HDACs and require oxidative stress

A) 90-8TLs were treated with vehicle, sapanisertib (100nM), vorinostat (2μM), or combined sapanisertib + vorinostat for 24 hours and a microarray analysis was performed. Gene sets related to oxidative or proteotoxic stress significantly altered in the combination treated cells relative to the other treatment groups (vehicle and monotherapies) are shown. The p-values for LS permutation, KS permutation, and Efron-Tibshirani GSA test for each gene set are shown, with p-values <0.005 highlighted in red. A complete list of the gene sets that were

recurrently differentially expressed is shown in Supplementary Table S1. **B)** Graph depicts relative mean fluorescence intensity of 90-8TL (black) and IMR-90 (gray) cells stained with dichlorofluorescin diacetate (DCFDA), a dye that measures reactive oxygen species (ROS) and treated as indicated for 48 hours (90-8TLs treated as in A, IMR90s treated as in Figure 1D). Error bars indicate SD from three technical triplicates. *p=0.002889, **p=0.000009 **C)** S462s were treated with vehicle, sapinsertib (200nM), vorinostat (2μM), or sapinsertib + vorinostat with (black) or without (white) 5mM N-acetyl cysteine (NAC). Left y-axis indicates log2 fold change in cell number after 3 days, The Log2 values on the left axis have been converted to the actual percent increase or decrease in cell number after 72 hours to best appreciate relative changes, shown on the right y-axis. Error bars indicate SD of technical triplicates. *p=0.009 D) S462s were treated as in C, immunoblot depicts phosphorylated S6 and acetylated histone H3 at lysine 9 after 24 hours of indicated treatments. Total S6 and vinculin serve as controls. **E)** Transmission electron microscopy (TEM) image of tumor cells after 7 hours of treatment with vorinostat and rapamycin. Red circles indicate representative endoplasmic reticulum (ER), and blue arrows indicate representative mitochondria (M). Scale bars are in white. **F)** S462s were treated with vehicle, buthionine sulfoximine (BSO, 200μM), vorinostat (2μM), or BSO + vorinostat. Left y-axis depicts log-2 fold change in cell number after 3 days. The Log2 values on the left axis have been converted to the actual percent increase or decrease in cell number after 72 hours to best appreciate relative changes, shown on the right y-axis. Error bars indicate SD of technical triplicates. *p =0.000003, **p<0.000001 G) Waterfall plot depicting log2 fold change in tumor volume after 10 days of treatment with buthionine sulfoximine (BSO, black) or BSO + panobinostat. The Log2 values on the left axis have been converted to the actual percent increase or decrease in tumor volume to best appreciate relative changes, shown on the right y-axis. Vehicle and sapinsertib + panobinostat data (grey) are reprinted from figure 1J for clarity. As in 1J, " * " denotes tumor that was undetectable by palpation at 10 days. Tumor size was determined by measuring residual flat lesion/tissue after dissection. **H)** S462s over-expressing either LACZ (white) or G6PD (black) were treated with vehicle or sapinsertib (200nM) + vorinostat (2μM). Left y-axis indicates log2 of fold change in cell number after three days. The Log2 values on the left axis have been converted to the actual percent increase or decrease in cell number after 72 hours to best appreciate relative changes, shown on the right y-axis. At right, immunoblot depicts G6PD after 16 hours of treatment with sapanisertib and vorinostat. Actin serves as a control. *p=0.000875

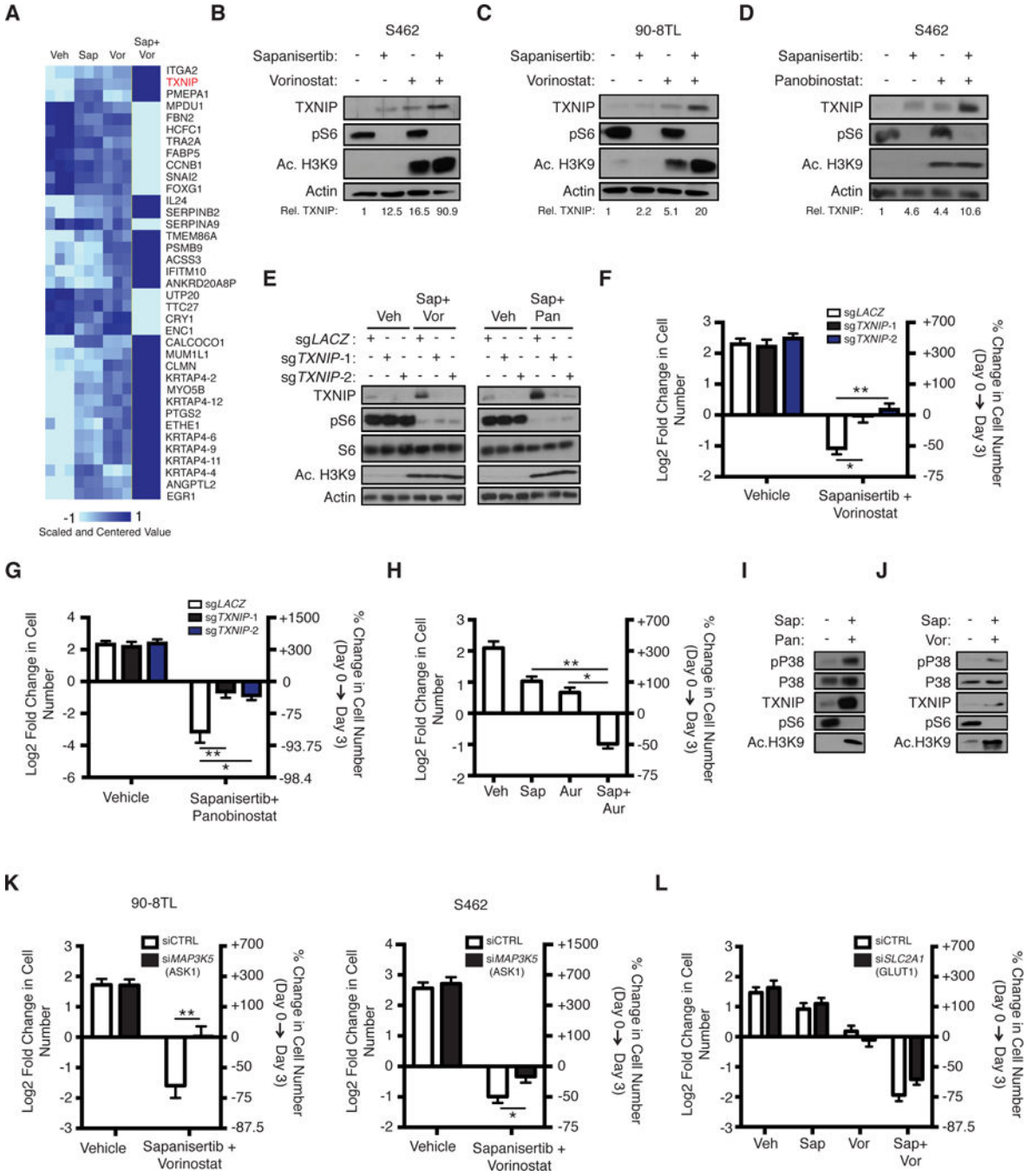

Figure 3. HDAC and mTOR Inhibitors function by converging on the Thioredoxin Interacting Protein (TXNIP) and activating Apoptosis Signal-regulating kinase 1 (ASK1)

A) Microarray analysis of 90-8TLs after 24 hours of treatment with vehicle, sapanisertib (100nM), vorinostat (2μM), or both sapanisertib and vorinostat. Heatmap depicts the uniquely upregulated genes (dark blue) or downregulated genes (light blue) from cells treated with sapanisertib plus vorinostat, as compared with all other treatment groups, with a $p < 0.001$ and a fold change of 1.5 or more. *TXNIP* is highlighted in red, as a gene of particular interest within this signature. **B)**. Immunoblot depicts protein levels of TXNIP,

phosphorylated S6 and Acetylated H3K9 after 16 hours of treatment with sapanisertib (200nM), vorinostat (2μM), or sapanisertib and vorinostat in S462s. Actin serves as a control. Below, numbers indicate relative TXNIP protein levels quantified and normalized to actin levels, with vehicle levels set to 1. **C)** 90-8TLs were treated with sapanisertib (100nM), vorinostat (2μM), or sapanisertib and vorinostat and analyzed as in B. **D)** S462s were treated with vehicle, sapinsertib (200nM), panobinostat (20nM), or sapinsertib + panobinostat and analyzed as in B. **E)** S462s were infected with lentiCRISPRv2 expressing guides against *LACZ* or *TXNIP* as indicated. Immunoblot depicts TXNIP, phosphorylated S6 (pS6), and acetylated histone H3 at lysine 9 (Ac. H3K9) protein levels after 16 hours of treatment as in B and D. Actin and S6 serve as controls. **F)** As in E, S462s were infected with lentiCRISPRv2 expressing guides against *LACZ* or *TXNIP* as indicated and treated with sapanisertib (200nM) and vorinostat (2μM). Left y-axis indicates the log2 of fold change in cell number after 3 days. The Log2 values on the left axis have been converted to the actual percent increase or decrease in cell number after 72 hours to best appreciate relative changes, shown on the right y-axis. Error bars indicate SD of technical triplicates.*p=0.000007, **p<0.000001 **G)** S462s with indicated CRISPR guides were treated with vehicle or sapinsertib (200nM) + panobinostat (20nM), and analyzed as in E. *p=0.000004, **p=0.000001 **H)** 90-8TLs were treated with vehicle, sapinsertib (100nM), auranofin (750nM) or auranofin + sapinsertib. Left y-axis indicates the log2 of fold change in cell number after 3 days. The Log2 values on the left axis have been converted to the actual percent increase or decrease in cell number after 72 hours to best appreciate relative changes, shown on the right y-axis. Error bars indicate SD of technical triplicates. *p=0.000004, **p<0.000001 **I)** Immunoblot depicting phosphorylated P38, TXNIP, acetylated histone H3K9, and phosphorylated S6 levels in S462s after 16 hours of treatment with sapanisertib (200nM) and panobinostat (20nM). P38 serves as a control **J)** Immunoblot depicting phosphorylated P38, TXNIP, acetylated histone H3K9, and phosphorylated S6 levels in 90-8TLs after 16 hours of treatment with sapanisertib (100nM) and vorinostat (2μM). P38 serves as a control **K)** 90-8TLs (left) and S462s (right) were transfected with pooled siRNAs targeting *MAP3K5* (ASK1) or non-targeting (CTRL) and treated with vehicle, sapanisertib (100nM 90-8TL, 200nM S462), vorinostat (2μM), or sapanisertib and vorinostat. Left y-axis indicates the log2 of fold change in cell number after 3 days. The Log2 values on the left axis have been converted to the actual percent increase or decrease in cell number after 72 hours to best appreciate relative changes, shown on the right y-axis. Error bars indicate SD of technical triplicates. *p=0.003935, **p<0.000001 **L)** 90-8TLs were transfected with pooled siRNAs targeting *SLC2A1* (GLUT1) or non-targeting (CTRL), and treated with vehicle, sapanisertib (100nM), vorinostat (2μM), or sapanisertib and vorinostat. Left y-axis indicates the log2 of fold change in cell number after 3 days. The Log2 values on the left axis have been converted to the actual percent increase or decrease in cell number after 72 hours to best appreciate relative changes, shown on the right y-axis. Error bars indicate SD of technical triplicates.

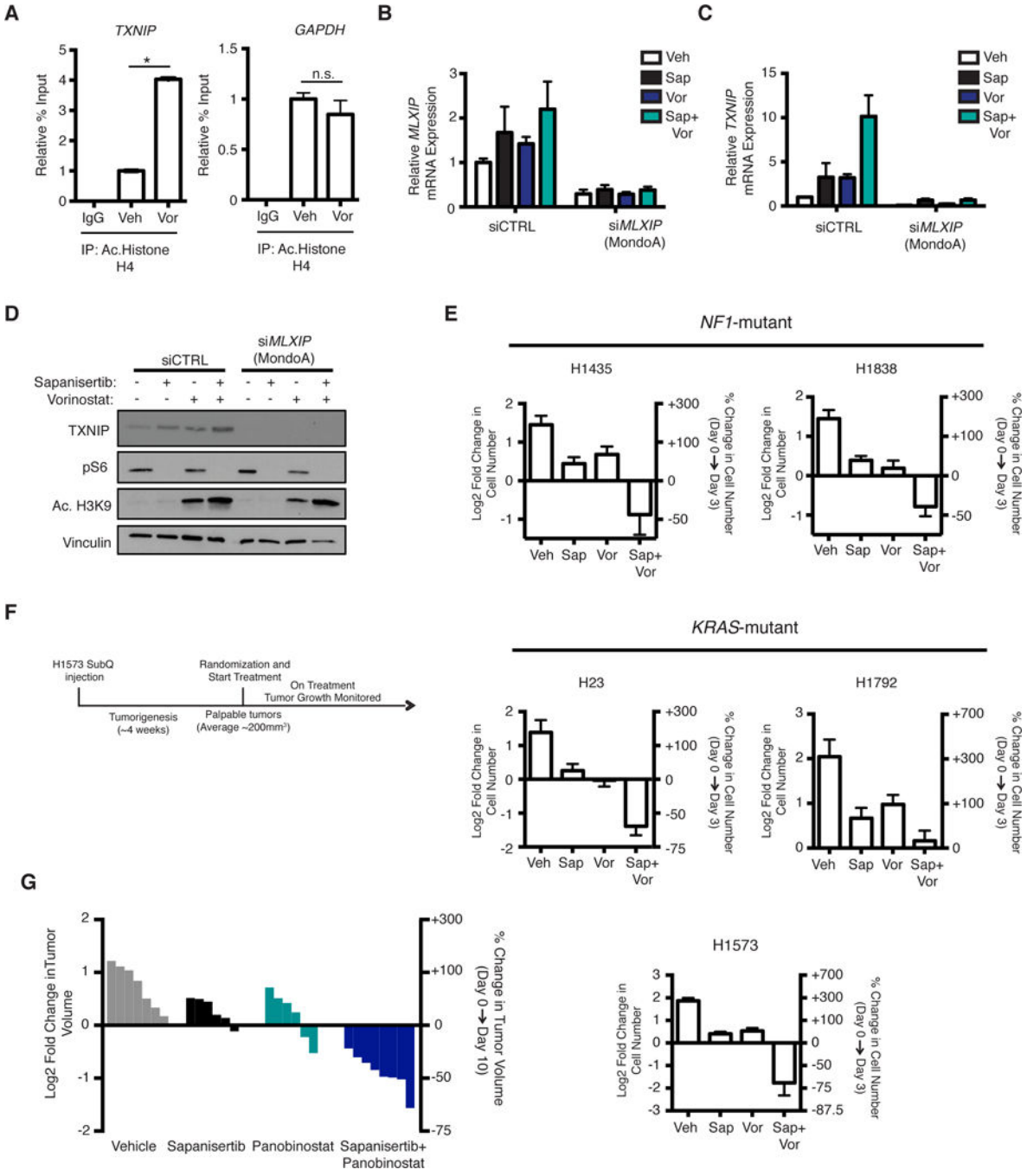

Figure 4. TXNIP expression is induced through cooperative effects on chromatin and transcription

A) 90-8TLs were treated with vehicle or vorinostat for 6 hours. Graph shows percent input of *TXNIP* (left) and *GAPDH* (right) relative to respective vehicle treatments, after chromatin immunoprecipitation of acetylated histone H4. IgG chromatin immunoprecipitation is shown as a control. **p*<0.0001 **B)** 90-8TLs were transfected with pooled siRNAs targeting *MLXIP* (MondoA) or non-targeting (CTRL), and treated with vehicle, sapanisertib (100nM), vorinostat (2μM), or sapanisertib and vorinostat. Graph depicts quantitative PCR of *MLXIP*

transcript levels in indicated treatment condition, 72 hours after transfection with indicated siRNA, and 24 hours after indicated treatment. Data points indicate relative mRNA expression, ± SD of three replicates. **C)** Cells were transfected and treated as in B, graph depicts quantitative PCR of *TXNIP* transcript levels in indicated treatment condition, 72 hours after transfection with indicated siRNA, and 24 hours after treatment as in B. Data points indicate relative mRNA expression, ± SD of three replicates. **D)** Immunoblot depicts TXNIP, phosphorylated S6 (pS6), and acetylated lysine 9 of histone H3 (Ac.H3K9) in 90-8TLs 72 hours after transfection with indicated siRNA and 24 hours after treatment as in B. Vinculin serves as a control. **E)** Indicated human NSCLC cells were treated with vehicle, sapanisertib (200nM), vorinostat (2μM), or sapanisertib and vorinostat. Graphs depict the percent change in cell number, relative to day 0 ±SD, on a log2 scale. *NF1* and *KRAS* mutation status is noted. **F)** Diagram of *in vivo* experimental design. **G)** Waterfall plot depicting change in tumor volume after 10 days of treatment with single and combined agents as indicated. *KRAS*-mutant xenografts (H1573 cells) were used for this analysis. Percent change in tumor volume after 10 days is graphed on a log2 scale. Each bar represents an individual tumor.

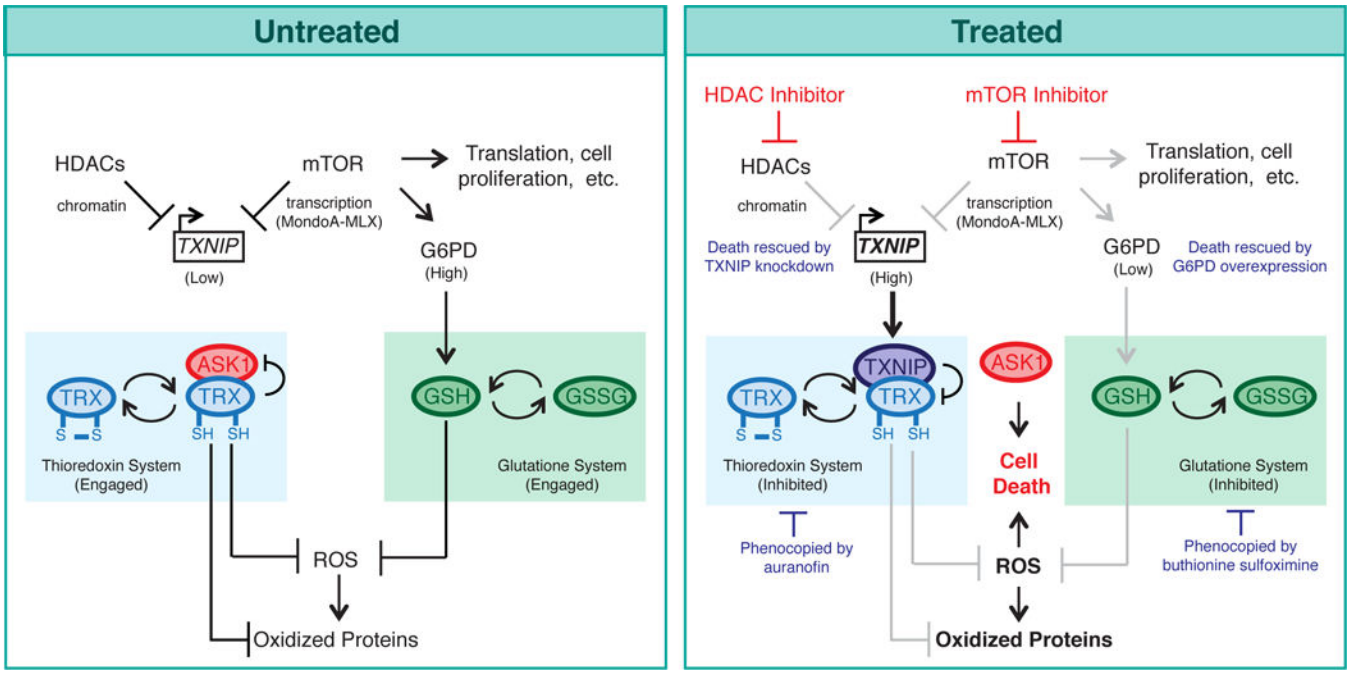

Figure 5. Model depicting the mechanism by which HDAC and mTOR inhibitors promote catastrophic oxidative stress and kill tumor cells

HDAC and mTOR inhibitors trigger irresolvable oxidative stress and cell death, by converging on two of the three major anti- oxidant pathways and activating ASK1. Specifically, as single agents mTOR inhibitors suppress the glutathione pathway, through effects on G6PD (17,18). However when combined with HDAC inibitors, these agents together induce TXNIP expression through cooperative effects on chromatin and the MondoA-MLX transcriptional complex. Importantly, TXNIP inhibits a second major antioxidant pathway in tumors (thioredoxin) and triggers ASK1 activation and together these events cause catastrophic oxidative stress, cell death, and tumor regression. This model is supported by both gain and loss-of-function studies. TXNIP ablation, G6PD overexpression (and ROS scavengers) all prevent cell death. Moreover, thioredoxin suppression can be phenocopied by auronofin, and glutathione suppression can be phenocopied by BSO.